



Assessing the Bendability of Ultra-High Strength Steel in Plane Strain Conditions

Phillip Krawec¹(✉), Sumit Hazra¹, Ed Bramberly¹, Bin Xiao², and Didier Farrugia²

¹ University of Warwick, Coventry, UK
phillip.krawec@warwick.ac.uk

² Tata Steel UK R&D, 9 Sir William Lyons Road, Coventry CV4 7EZ, UK

Abstract. Inconsistent behavior and premature failure are common when bending Ultra-High strength steels (UHSS). Practicality limits laboratory testing to smaller samples, which may not replicate the conditions of production or result in plane strain loading, and larger volumes of material used in manufacturing may increase the likelihood that material inhomogeneities will cause failure.

A rig was developed, capable of replicating the size and scale of production. Tests have been undertaken on a commercial grade of UHSS at 5 forming radius/thickness ratios with strains measured using digital image techniques. Results show that punch separation occurs on specimens that ultimately fail, causing bend severity to increase unexpectedly. This occurs at consistent bending punch displacements during the bending process, with initial bending strains matching until a deviation point. Clear visual separation was observed to occur more frequently when the line along which the material was bent was parallel to its rolling direction than when it was perpendicular. Upcoming investigations will focus on behavior at this deviation point to try and better understand this separation. Understanding of this phenomenon may increase suitable applications for UHSS when bend forming is required.

Keywords: Bendability · Ultra-high Strength Steel · Formability · Digital Image Correlation

1 Introduction

Plane strain bending, as present with a suitably wide sample in the bending direction, has a unique loading condition that differs from that of other forming operations. While in plane strain bending, there is a strain gradient, resulting in pure tensile stress at the external bending face, and pure compressive stress at the internal bending face [1].

The forming limit diagram (FLD) is a commonly used tool in manufacturing to describe the strains that a material can undertake before failure. Unfortunately, the forming limit curve is unable to predict failure in bending due to differences in failure mechanisms – the forming limit curve predicts membrane instability, the onset of necking, while bending failures occur due to ductile shear in the outer bending edge, the outer edge in tension. To better assess the unique conditions found under bending conditions, Schleich describes an alternative diagram for assessing bendability – the Bending

Limit Diagram (BDL). The BDL is determined based on the critical strain to failure at varying pretension loads and inner bending radii and was effective at predicting failure for deep-drawing and hemming operations with small bending radii [2, 3].

Bendability of Ultra-High strength steels (UHSS), as defined by having a minimum tensile strength ≥ 780 MPa, may be limited due to issues around “punch-sheet separation”, sometimes referred to as “kinking” [4] or “Multi-breakage” [5]. During this phenomenon, the bending punch and sheet separate during bending, resulting in 4 points of contact on the sheet, and an inner bend radius smaller than that of the punch. This causes 2 main issues: geometric inconsistency of manufactured parts due to the unpredictable discrepancy between the punch radius and the finished sheet bend radius, and an increase in strain and possible premature failure due to the reduced bend radius [4, 6, 7]. This phenomenon has been observed throughout literature [5, 6, 8], and the exact reasoning behind the separation is not fully explained, however observations include increased strain localization over a smaller bending width [5, 9]. The behavior may be more common when using a larger punch size [10], as used in the following experiments. Modelling of the separation phenomenon is rare, but has been considered [11, 12].

Anisotropic behavior of UHSS is also common, resulting in limited bendability when bending in certain directions in respect to the rolling direction. Decreased performance when bending parallel to the rolling direction is common [9], causes of which may include subsurface microstructural composition combined with strong shear textures [13, 14]. This anisotropic behavior may also limit the final applications due to constraints on geometries.

Digital Image Correlation (DIC) has been used extensively in bending analysis; however, focus is generally on the outer bending face [5, 15–17]. In the following experiments, focus has been on the through-thickness edge of the material. Experiments also focus on larger specimens than generally used in laboratory testing to better simulate production conditions, with a minimum thickness to width ratio of 50:1 tested.

2 Experimental Setup

2.1 Tested Material

Testing took place on a commercially available grade of UHSS with a primarily martensitic structure, unnamed for commercial reasons. Table 1 gives the typical chemical composition. Typical mechanical properties were determined using tensile testing. The material was supplied from production cut-to-length sheets from the hot strip mill.

Table 1. Target elemental composition for the commercial grade of UHSS used, % by weight.

C	Mn	P	S	Si	Al	Nb
≤ 0.12	≤ 1.8	≤ 0.02	≤ 0.003	≤ 0.15	≥ 0.015	≤ 0.05
V	Ti	Mo	B	Ni	Cr	
≤ 0.15	≤ 0.05	≤ 0.5	≤ 0.005	≤ 0.1	≤ 0.6	

2.2 Tensile Testing

Tensile testing was undertaken using an Instron 150 kN Universal Testing Machine, tested to BS EN ISO 68925-1:2019 at a set displacement speed of 2 mm/min [18]. The test piece geometry had a gauge length of 50 mm, gauge width of 12.5 mm and total length of 200 mm. Testing took place in 3 directions, 0°, 45°, and 90° to the rolling direction. Tests were undertaken on 3 thicknesses of material: 4 mm, 5 mm, and 6 mm. 5 repeats were done for each direction for each thickness.

2.3 Bending Tests and Digital Image Analysis

Bending tests were undertaken on a newly developed rig placed on an Interlaken 1000 kN hydraulic double-action press, developed as part of a previous WMG-Tata Steel Catapult project [19]. The rig consists of 2 functional sections: an upper section containing the selectable punch assembly, and a lower section featuring the selectable butterfly die.

The upper section allows for a selectable punch size and shape to be used for the bend tests. A machined T-slot is used to facilitate punch switching. Tests described in this paper took place using 3 circular punch sizes: with a radius of R15, R20 and R25.

The lower assembly consists of a hardened steel “butterfly” arrangement V-die. This allows the testing of different bending configurations. Tests described in this publication took place using the large die only. The large die used in the bend tests uses 8 mm radii bend supports with a 100 mm separation between supports. Figure 1 shows the die arrangement and dimensions. The test bed of the lower assembly is 400 × 400 mm, allowing up to 400 mm full contact bending. During testing, the upper punch assembly remains stationary, while the butterfly die moves upwards into the stationary punch.

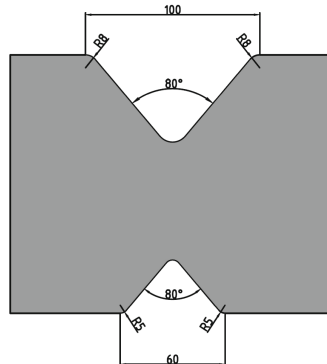


Fig. 1. Dimensions of the “Butterfly” V-die configuration. Only results from the larger die (top) are presented here.

Test specimens featured a bend length of between 300–310 mm to ensure the plane strain conditions by sample length being > 10x the specimen thickness as stipulated in BE EN ISO 7438:2020 [20]. The thickness-length ratio is a minimum of 75, 60, and 50 for the 4 mm, 5 mm and 6 mm specimens respectively.

Bend tests took place to ensure a range of strains and bending configurations, using each of the R15, R20 and R25 punches and 4 mm, 5 mm, and 6 mm sheet thicknesses. Tests took place bending both parallel and perpendicular to the rolling direction. The tests were undertaken at a punch displacement rate of 0.1 mm/s to ensure quasistatic conditions and allow for adequate frame capture rate for the DIC equipment without blurring or loss of focus. Bending specimens were tested in the “as received” condition in regard to the surface condition.

Edge strain, displacement, and bending angle were measured using GOM ARAMIS 12M Digital Image Correlation (DIC) equipment. The stochastic speckle pattern was applied to the outer edge of the sheet during the bending test – allowing through test analysis of the strains and displacement throughout the bending test. The painted edge was prepared with 120 Grit to ensure a plane edge suitable for paint adhesion. No further preparation was deemed necessary, as no decohesion of the paint, or edge cracking was observed during testing. The speckle pattern was also applied to the punch to assess any potential punch deformation and to locate the punch during analysis. Strains on the sheet faces were measuring using the GOM ARGUS Circle Grid Analysis (CGA) method. As the die is enclosed and unable to be observed during the test, the strains measured are taken after the test, after springback and bending has taken place. The circle grid pattern was applied prior to the bend test using a stencil and applied with white spray paint. The pattern consists of 2 mm diameter circles with a 3 mm center-center spacing. Figure 2 shows the location and application of each of the painting patterns.



Fig. 2. Application of paint patterns for strain analysis. A speckle pattern is applied to the edge and bending punch for DIC analysis, while the circle pattern is applied to the face for CGA analysis.

3 Results

3.1 Tensile Testing

Results from tensile testing shows anisotropic behavior from the material, with higher yield and tensile strength, but lower uniform and total elongation, when tested perpendicular to the rolling direction. Total elongation was considerably lower when testing specimens perpendicular to the rolling direction, with maximum stress dropping quickly from a maximum prior to fracture. Uniform elongation was generally lower for the 4 mm thickness compared to the other thicknesses. Table 2 shows the properties measured.

Table 2. Measured mechanical properties from tensile testing of the commercial grade of UHSS, 4 mm, 5 mm, and 6 mm thickness.

Property	4 mm			5 mm			6 mm		
	0°	45°	90°	0°	45°	90°	0°	45°	90°
Yield Strength (YS)/MPa	1085	1131	1175	1117	1129	1147	1087	1132	1166
Tensile Strength (UTS)/MPa	1183	1230	1240	1231	1239	1259	1193	1207	1251
Uniform Elongation/%	3.23	2.73	1.96	3.33	2.79	2.62	3.36	2.76	2.25
Total Elongation/%	8.97	8.57	4.96	10.73	10.04	8.41	11.44	10.93	6.50

3.2 Bending Tests and Digital Image Analysis

Punch-sheet separation was observed in all thicknesses and all test directions, both bending parallel and perpendicular to the rolling direction. Clear visual separation was more common when the bend line was parallel to the rolling direction, occurring on 75% specimens tested in this direction, in comparison to 33% occurrence when bending perpendicular to the rolling direction. Figure 3 shows the phenomenon of punch-sheet separation. Figure 4 shows the DIC strain distribution comparison at maximum punch displacement. When separation occurs, higher strains are localized within a smaller area below the punch.

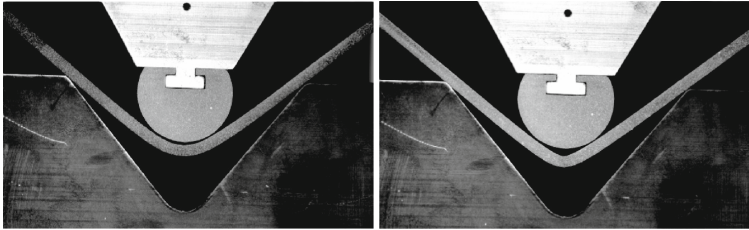


Fig. 3. Visual representation of punch-sheet separation. Each photograph shows the same bend conditions and material. Left shows the specimen wrapped around the punch in an ideal scenario. Right shows punch-sheet separation, with a gap appearing underneath the center of the punch. 5 mm thickness, R20 punch.

The maximum strain at the sheet edge for 5 mm specimens is shown in Fig. 5, repeated 8 times. Sheets that did not show separation reached a maximum strain average of 17.8%. Sheets that did separate from the punch showed considerably higher strains, with a greater range from between 26.8% to 40.3%.

Figure 6 shows the maximum strain on the sheet edge, as measured using DIC, for the 4 mm specimens (R15 Punch) as a comparison between a specimen that did and did not display punch-sheet separation. Each specimen shows increasing strain till the end of the test, but separation increased the final maximum strain. The maximum strain between the two specimens matched until a deviation point at approximately 21 mm punch displacement.

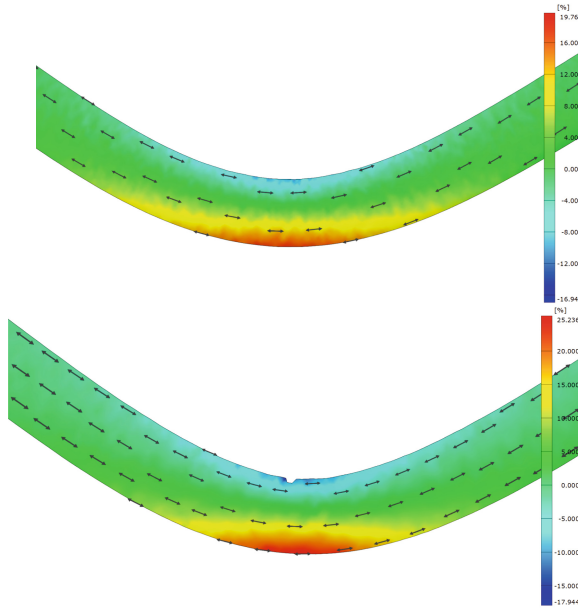


Fig. 4. Strain distribution at maximum punch displacement from DIC. 5 mm sheet thickness and R20 punch. TOP: Strain distribution for specimen not displaying punch-sheet separation. BOTTOM: Strain distribution for specimen displaying punch-sheet separation. The missing notch in the center is due to an unresolved section, as opposed to damage or cracking.

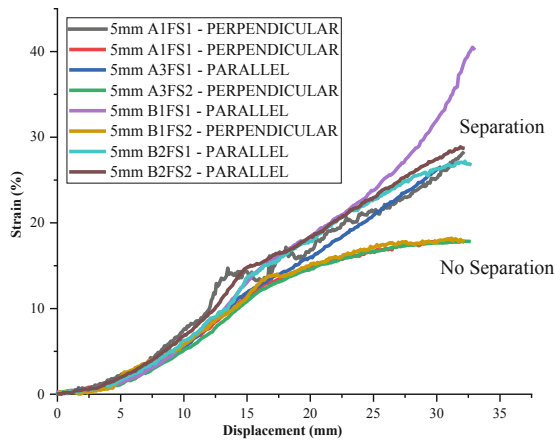


Fig. 5. Maximum strain measured on the sheet edge for 5 mm thickness specimens tested with the R20 punch. Specimens that showed separation reached higher strains. Specimens that did not separate averaged at a maximum of 17.8% at maximum punch displacement.

Figure 7 shows the comparison between punch-sheet separation and a specimen that did not show the phenomenon for 6 mm thickness tested with R25 punch. Maximum

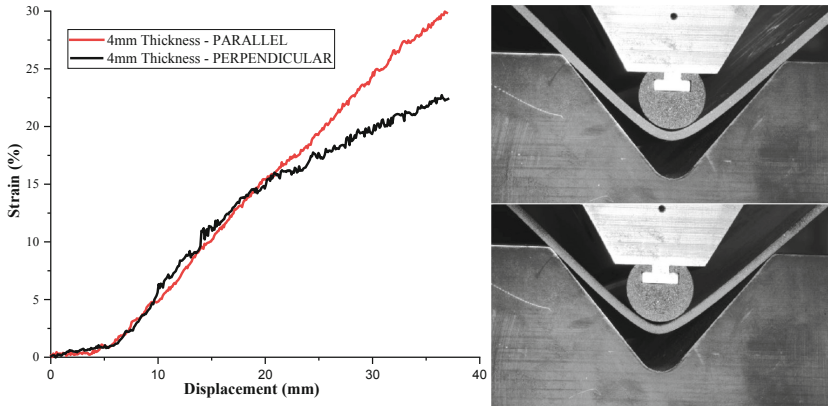


Fig. 6. LEFT: 4 mm specimens tested with R15 punch; specimen presented in red showed clear visual punch-sheet separation. UPPER RIGHT: Specimen with the bend line perpendicular to the rolling direction not displaying punch-sheet separation. LOWER RIGHT: Specimen with the bend line parallel to the rolling direction displaying punch-sheet separation.

strains at low punch displacements were consistent between specimens until a deviation point at a punch displacement of approximately 11 mm. Each specimen plateaued at a maximum strain at a punch displacement of approximately 28 mm, but with a higher maximum strain recorded on the specimen displaying punch-sheet separation.

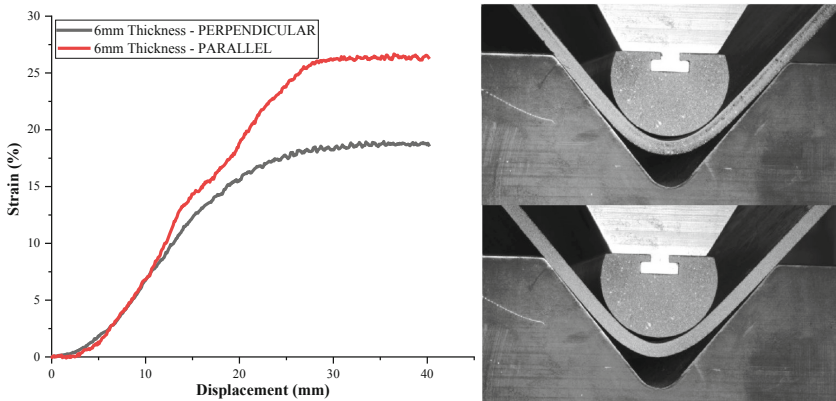


Fig. 7. LEFT: 6 mm sheets tested with R25 punch. Specimen presented in red showed punch-sheet separation, while specimens displayed in black did not. UPPER RIGHT: DF27A2 FS2 specimen not displaying punch-sheet separation. LOWER RIGHT: DF27A5 FS1 specimen displaying punch-sheet separation.

Table 3 shows the number of specimens that clear visual displayed punch-sheet separation during the bend test, and the direction in which bending took place in regard to the rolling direction. All test conditions, in all bending directions, showed punch-sheet separation on some specimens. However, the occurrence was more common when the

bend line was parallel to the rolling direction. Due to the number of repeats, the 5 mm thickness material with the R20 punch is thought to be most statistically representative from this batch of experiments. Other punch sizes and thicknesses tested used a greater range of final displacements, including low displacements at which separation may not have had a chance to develop fully. Further work will focus on repeating the R15 and R25 tests at higher displacements for confirmation.

Table 3. Percentage of specimens displaying clear visual separation between the punch and sheet for each tested punch radius and sheet thickness in regard to the bend direction relative to the material rolling direction.

Thickness	4 mm		5 mm		6 mm	
	Bend direction		Bend direction		Bend direction	
Former Radius/mm	Parallel	Perpendicular	Parallel	Perpendicular	Parallel	Perpendicular
15	50%	50%	—	—	50%	50%
20	—	—	100%	25%	—	—
25	25%	0%	—	—	100%	50%

4 Discussion and Future Work

The development of punch-sheet separation during the forming process causes issues of premature failure and geometric inaccuracies from target dimensions resulting in rejection of parts and increased costs. The clear visual separation occurred more often when bending parallel to the rolling direction. When bending in this direction, tensile force on the outside of the sheet is applied at 90° to the rolling direction.

Typically, the strain values, as measured using the DIC equipment, were consistent between specimens at low strain values. The 5 mm thickness results tested with the R20 punch (Fig. 5), show consistency between all specimens until a punch displacement of approximately 14 mm is reached, or a strain of approximately 10%. After this value, further punch displacements result in considerably increased strain for specimens that show clear visual separation. Early consistency with measured strain, followed by deviation at higher punch displacements was also observed in both the 4 mm and 6 mm specimens. Such behavior has been observed in other studies previously at low bending angles [5].

Characterization of the material throughout a range of strains is required to determine the behavior of the material as strain is increased. To this end, undertaken bends will be sectioned and subject to hardness analysis throughout the bending radius and microscopic analysis for further investigations into strain distribution, damage accumulation and possible microstructural effects, with a comparison being made to other published works regarding the onset of strain localization and damage mechanisms [4].

5 Conclusion

- a) Digital Image Correlation is a suitable and effective technique for characterizing strain and bending angles and displacements while using a sufficiently thick sheet.
- b) Tensile data showed significant anisotropic behavioural differences between 0° and 90° material – echoed by the differences in bending performance.
- c) Punch-sheet separation causes premature failure and geometric inaccuracies.
- d) In the material tested, punch-sheet separation occurred more frequently while bending parallel to the rolling direction. This suggests, along with the tensile data, that anisotropic material behavior is present.

Acknowledgements. The author would acknowledge the financial support of Tata Steel UK, with additional input from Bin Xiao and Didier Farrugia.

References

1. Hosford, W.F.: Metal forming: mechanics and metallurgy - chapter 13: bending. In: Cad-dell, R.M., Hosford, W.F. (eds.) *Metal Forming: Mechanics and Metallurgy*, pp. 199–211. Cambridge University Press, Cambridge (2011)
2. Schleich, R., Sindel, M., Liewald, M.: Investigation on the effect of curvature on forming limit prediction for aluminium sheet alloys. *Int. J. Mater. Form.* **2**(2), 69–74 (2009)
3. Schleich, R., et al.: Investigation on the effect of curvature and sheet thickness on forming limit prediction for aluminium sheet metal alloys. *Int. J. Mater. Form.* **2**(S1), 411–414 (2009)
4. Arola, A.M., et al.: The effect of mechanical behavior on bendability of ultrahigh-strength steel. *Mater. Today Commun.* **26** (2021)
5. Pokka, A.-P., et al.: Strain distribution during air bending of ultra-high strength steels (2021)
6. Wagner, L., et al.: Improved bendability characterization of UHSS sheets. In: Van Den Boogaard, T., Hazrati, J., Langerak, N. (eds.) *38th International Deep Drawing Research Group Annual Conference (IDDRG 2019)* (2019)
7. Kesti, V., et al.: Bendability and microstructure of direct quenched optim 960QC. *MSF* **783–786**, 818–824 (2014)
8. Ruoppa, R., et al.: Bending properties of some ultra-high-strength steels, p. 10. Kuldeep Viridi and Lauri Tenhunen (Editors) (2012)
9. Ruoppa, R., et al.: Bendability tests for ultra-high-strength steels with optical strain analysis and prediction of bending force, p. 68. Kuldeep Viridi and Lauri Tenhunen (Editors) (2014)
10. Vorkov, V., et al.: Experimental investigation of large radius air bending. *Int. J. Adv. Manuf. Technol.* **92**(9), 3553–3569 (2017)
11. Pourboghrat, F., Stelson, K.A.: Pressbrake bending in the punch-sheet contact region—part 1: modeling nonuniformities. *J. Eng. Ind.* **110**(2), 124–130 (1988)
12. Pourboghrat, F., Stelson, K.A.: Pressbrake bending in the punch-sheet contact region—part 2: gap formation and the direction of sheet motion. *J. Eng. Ind.* **110**(2), 131–136 (1988)
13. Saastamoinen, A., et al.: The effect of thermomechanical treatment and tempering on the subsurface microstructure and bendability of direct-quenched low-carbon strip steel. *Mater. Charact.* **134**, 172–181 (2017)
14. Kaijalainen, A.J., et al.: Influence of composition and hot rolling on the subsurface microstructure and bendability of ultrahigh-strength strip. *Metall. Mater. Trans. A.* **47**(8), 4175–4188 (2016)

15. Arola, A.-M., et al.: Digital image correlation and optical strain measuring in bendability assessment of ultra-high strength structural steels. *Procedia Manuf.* **29**, 398–405 (2019)
16. Cheong, K., Butcher, C., Dykeman, J.: The influence of the through-thickness strain gradients on the fracture characterization of advanced high-strength steels. *SAE Int. J. Mater. Manuf.* **11**(4), 541–552 (2018)
17. Noder, J., Dykeman, J., Butcher, C.: New methodologies for fracture detection of automotive steels in tight radius bending: application to the VDA 238–100 V-bend test. *Exp. Mech.* **61**(2), 367–394 (2021)
18. BSI: BS EN ISO 6892-1:2019 Metallic Materials - Tensile Testing Part 1: Method of Test at Room Temperature (2019)
19. Mitchell, A., Pakiyaraja, N.: University of Warwick Secondment: Bending of Valast® 450 for Engineering Sector, Tata Steel - WMG Catapult Project: Tata Steel (2021)
20. BSI: BS EN ISO 7438:2020 Metallic Materials - Bend Test. BSI. p. 20 (2020)